Geoscience Frontiers 12 (2021) 255–263

HOSTED BY

Contents lists available at ScienceDirect

Geoscience Frontiers

journal homepage: www.elsevier.com/locate/gsf

Research Paper

Sicilian serpentinite xenoliths containing abiotic organics with nanodiamond clusters as key model for prebiotic processes

Sergei K. Simakov [a,*], Vittorio Scribano [b], Nikolai N. Mel'Nik [c], Germana Barone [b]

[a] LLC "ADAMANT" Skolkovo Participant, Tikhoretsky 10/1-61, St.Petersburg, 194064, Russia
[b] Department of Biological, Geological and Environmental Sciences, University of Catania, Corso Italia 55-I-95129 Catania, Italy
[c] Lebedev Physics Institute, Russian Academy of Sciences, Leninsky Pr. 53, Moscow, 119991, Russia

ARTICLE INFO

Handling Editor: Vinod Oommen Samuel

Keywords:
Hydrothermal systems
Nanocarbons
Sulfides
FT-t synthesis
Abiogenesis
LUCA, Sicily
Micro-Raman

ABSTRACT

Rock fragments from the deepest parts of a buried hydrothermal system belonging to the Mesozoic Tethys Ocean entered as xenoliths in a Miocenic diatreme, hence brought to the surface, in the Hyblean Plateau (Sicily). Some xenoliths consist of strongly serpentinized ultramafic rocks bearing blebs of abiotic organic matter, where clusters of amorphous carbon nanoparticles, including nanodiamonds, are immersed. Such an occurrence conjures up established hypotheses that diamond surfaces are suitable catalytic platforms stimulating the assemblage of complex bio-organic molecules relevant to the emergence of life on Earth. The appearance of bio-organic molecules under primitive Earth conditions is one of the major unsolved questions on the origin of life. Here we report new micro-Raman spectra on blebs of abiotic organic matter from a selected xenolith. Diamond bands were related to hydrogenated nanocrystalline diamonds, with size of nearly 1–1.6 nm, formed from organics at low pressures and temperatures. In particular, diamond surfaces can give rise to crystalline interfacial water layers that may have played a fundamental role in the early biosphere evolution as a good medium for rapidly transporting positive charges in the form of hydrated protons. Nowadays, proton gradients in alkaline hydrothermal vents along oceanic ridges are generally viewed as key pre-biotic factors. In general, serpentinites span the entire geological record, including prebiotic times. These hydrous ultramafic rocks often display evidence of abiotic carbon species, both organic and inorganic, including nanodiamonds, being also capable to give rise to chemiosmotic processes and proton gradients necessary to the organisms, such as the "Last Universal Common Ancestor" (LUCA), in the prebiotic Earth.

1. Introduction

Serpentinite-hosted hydrothermal systems are ideal places for abiotic synthesis of organic compounds, both gaseous and condensed, generally having low molecular weight (McCollom and Seewald, 2013; Mé;nez et al., 2018). In addition, serpentinite systems favour the formation of a number of redox-sensitive minerals, such as sulfides, whose surfaces are capable of binding simple organic molecules, hence catalyzing different proto-biochemical reactions (Holm et al., 1993; Bebié and Schoonen, 2000; Wang et al., 2010). It has been therefore reasonable to consider serpentinite systems as ideal places for the emergence of life on the early Earth (e.g. Russell et al., 2005). In more recent geological times, molecular hydrogen, abiotic organic compounds and sulfur, produced during the multistage hydrothermal alteration of the oceanic crust, have provided energy sources for metabolic reactions of microbial ecosystems (e.g. Brazelton et al., 2011; Menéz et al., 2018 and references therein).

The abiogenic production of organic compounds (low-molecular-weight alkanes in most cases) in serpentinite-hosted hydrothermal systems is thought to occur via Fischer–Tropsch-type (FT-t) reactions (e.g. Konn et al., 2009):

$$n\mathrm{CO_2} + (3n{+}1)\mathrm{H_2} \rightarrow \mathrm{C}_n\mathrm{H}_{2n+2} + 2n\mathrm{H_2O} \quad (1)$$

Such a reaction, at molecular scale, can be viewed as a process catalyzed by diverse oxide minerals (e.g. magnetite, trevorite), native metals and alloys, formed as by-products of the serpentinization reactions (e.g. McCollom and Seewald, 2013).

Submarine hydrothermal systems in the prebiotic Earth have therefore had the "basic ingredients" required for the so-called

* Corresponding author. Tel.: +7 921 9608578.
E-mail address: sergei_simakov@yahoo.com (S.K. Simakov).
Peer-review under responsibility of China University of Geosciences (Beijing).

https://doi.org/10.1016/j.gsf.2020.04.008
Received 20 November 2019; Received in revised form 24 January 2020; Accepted 7 April 2020
Available online 24 April 2020

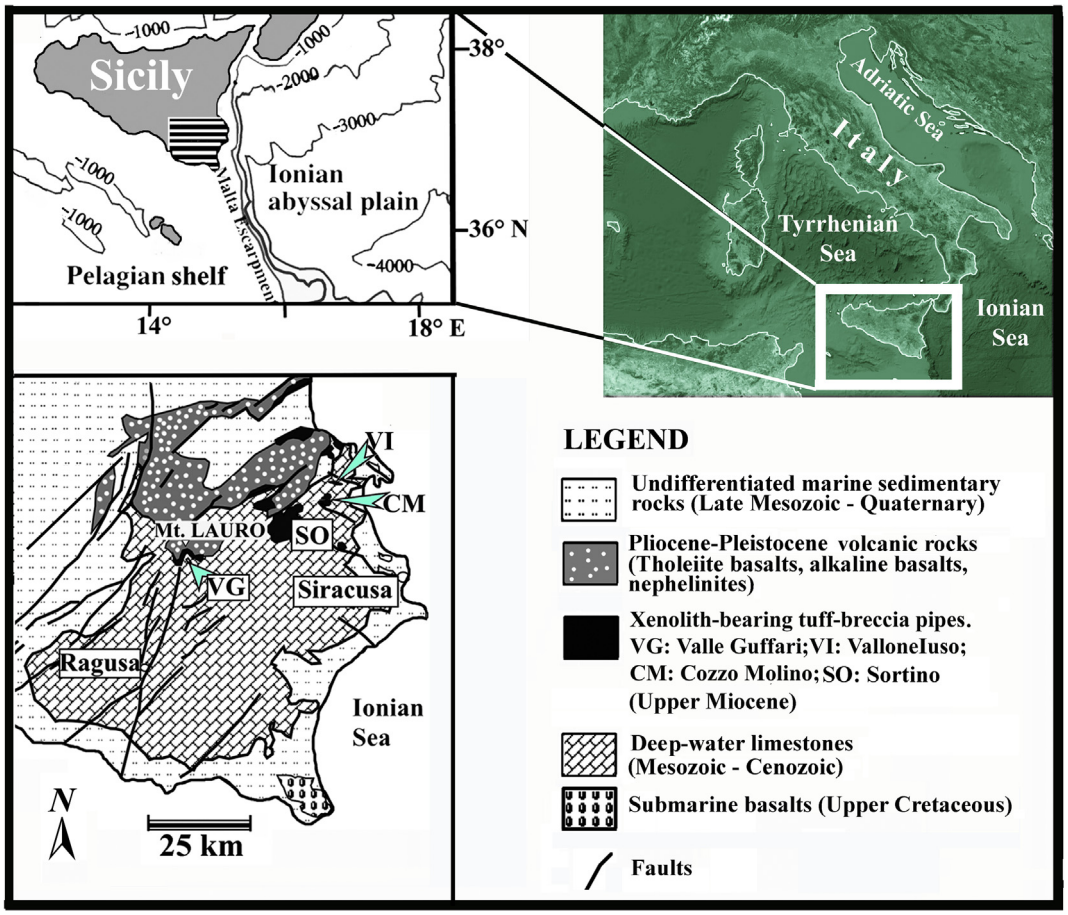

Fig. 1. Geological setting of the study area. The nanodiamond bearing sample has been recovered from the tuff-breccia deposit from Valle Guffari (VG in the figure).

chemoautotrophic origin-of-life scenarios, including an abundance of chemical energy sources and conditions conducive to the reduction of CO_2 to simple organic compounds. Cores of many enzymes involved in carbon fixation in extant chemosynthetic microorganisms contain Fe–S clusters, whose structure resembles the unit cell of sulfide minerals found in deep-sea hydrothermal-vent chimneys (Blöchl et al., 1992). This suggests the possibility that enzyme cores may represent remnants of the earliest stages of biochemical evolution. Geochemical gradients that developed at the interface between alkaline, H_2-rich hydrothermal fluids and mildly acidic CO_2-rich seawater would have provided sources of chemical energy for evolving metabolisms (Schulte and Rogers, 2004). Carbon dioxide and possibly other electron donors, such as SO_4^{2-}, would have been available to provide energy via reactions that include methano-*l* genesis and sulfate reduction (McCollom and Seewald, 2013). pH gradients may have been an additional source of metabolic energy in these environments (Lane et al., 2010). Proton gradients in alkaline hydrothermal vents are thought to be promoting conditions for the origin of life (Lane et al., 2010), as commonly observed in archea and bacteria. As expected, they generate proton gradients across cytoplasm membranes and conduct electrons and pump protons using ferredoxins, quinones and cytochromes (Baymann et al., 2003). Extant microorganisms gain metabolic energy by maintaining a proton gradient across membranes, and in serpentine-hosted submarine hydrothermal environments, including those likely occurred on early Earth, such gradients would evolve naturally at the interface between hydrothermal-vent fluids and seawater.

In addition to the essential role of mineral surfaces in the organic synthesis via FT-t pathway, surfaces of several mineral phases were also thought to be catalytic platforms stimulating the assemblage of complex bioorganic molecules relevant to the emergence of life on Earth (Holm et al., 1993; Bebié and Schoonen, 2000; Hazen and Sverjinsky, 2010). Carbon is considered an excellent platform for proto-biochemical reactions (Sommer et al., 2008). Surface conductivity on hydrogen-terminated polycrystalline CVD (chemical vapor deposition) diamond was first reported by Landstrass and Ravi (1989). It has been demonstrated that high concentration of hydrogen in the gas mixture is required to promote the formation of diamond bonds, as opposed to the equilibrium form of carbon, graphite (Spitsyn et al., 1981; Matsumoto et al., 1982; Fedoseev et al., 1984). Landstrass and Ravi (1989) have shown that the main movement of hydrogen within or out of the film, could occur at annealing temperatures as low as 100 °C. The diamond surface could create the crystalline interfacial water layers even at room temperature (Sommer et al., 2008). These layers would play a fundamental role in biology and evolution (Szent-Gyorgyi, 1971). They are also essential for the viability of bacteria (Webb, 1965). Life may have started with building such water structures (Szent-Gyorgyi, 1971) because these are a good medium for rapidly transporting positive charge in the form of hydrated protons (Sommer et al., 2008). In this respect, it is important to highlight that nanodiamonds are present in shallow Earth crustal rocks, whose formation is connected to organic matter and water including serpentinites (e.g. Simakov et al., 2015; Simakov, 2018 and references therein).

Nanodiamonds are carbon nanoparticles of enigmatic origin; they can be defined as the archetypal “macroscopic molecule” (Dahl et al., 2003). Hydrogen-terminated diamonds and nanometre-sized diamondoid hydrocarbons form a continuous structural series (Piekarczyk, 1999) including lower diamondoids (<1 nm), higher diamondoids (~1–2 nm), nanocrystalline and chemical vapor deposition (CVD) diamonds (~2 nm–1 μm), and macroscopic diamonds (Angus and Hayman, 1988; Ristein, 2001). Nanodiamonds are found also in chondrite meteorites (Dai

Table 1
Synoptic petrologic and geochemical information on the sample.

Sample label	Geographic coordinates	Sample type	Shape/Size		Secondary processes
G3	37°04′09.27″N 14°49′07.92″E Elv. 848 m	Ultramafic xenolith	Ovoid/~12 cm × 8 cm × 6 cm		Serpentinization carbonation
Mineral mode (~vol%)	**Mineral chemistry**				
	Cpx	Opx	Spl		Srp
Cc = 40	Wo = 45.5 mol%	9	Mg#	Cr#	SiO_2 = 43.2 wt.%
Srp = 33	En = 49.5 mol%	91.6	75 (Core)	35 (Core)	MgO = 43.5 wt.%
Cpx = 9	Fs = 5 mol%	7.5	70 (Rim)	43 (Rim)	H_2O = 12.8 wt.%
Opx = 8	Mg# = 90	92			
Spl = 4	Al_2O_3 = 3.9 wt.%	2.4			
OM = 4	Cr_2O_3 = 0.6 wt.%	0.3			
Others = 2	TiO_2 = 0.14 wt.%	0.03			

Whole-rock chemistry

Major elements (in wt.%)			Trace elements
	Actual	Volatile-free	
SiO_2	25.90	50.46	Cr = 2986 ppm
Al_2O_3	2.11	4.15	Ni = 1070 ppm
TiO_2	0.10	0.20	S = 1400 ppm
Fe_2O_3*	3.56	7.00	Zr = 6.3 ppm
MgO	15.40	30.22	Y = 2.5 ppm
$Na_2O + K_2O$	0.12	0.24	ΣREE = 23.2 ppm
L.O.I.	24.20	–	La/Yb = 39

Note: Cc = calcite; Srp = serpentine and its phyllosilicate retrograde products (chlorite/smectite interlayers); Cpx = clinopyroxene; Opx = orthopyroxene; Spl = spinel; OM = condensed organic matter; Others = sulfides (pyrite, pentlandite, millerite, galena), apatite, Fe-sulfate, sylvite.
Mg# = 100 Mg/(Mg + Fe^T); Cr# = Cr/(Cr + Al); Fe_2O_3* as total Fe^{3+}.

et al., 2002) and interplanetary dusts (Galli, 2010). These nanodiamonds are often associated with diamondoids (Bauschlicher et al., 2007). Astronomers concluded that 3% of the carbon present in meteorites is in diamond form and that 10%–20% of interstellar carbon exists in the form of ultrananocrystalline diamonds (Tielens et al., 1987). In addition, Kouchi et al. (2005) related interstellar diamond formation to water and organic matter. As expected, radio-astronomy observations have detected many other compounds coexisting with nanodiamonds, such as hydroxyl OH, water and ammonia vapors, formaldehyde, carbon monoxide, methanol (wood alcohol), ethyl (wine) alcohol, and dozens of other more complex organic molecules in interstellar clouds (e.g. Nakano et al., 2002).

On Earth, remarkable amounts of diamondoids occur in crude oils and gas condensates (from 35 ppm to 2075 ppm, respectively; e.g. Nekhaev et al., 2011). In this respect, it is worth to recall that fragments of serpentinites from the deepest parts of a buried hydrothermal system belonging to the Mesozoic Tethys Ocean lithosphere entered as xenoliths in a Miocenic tuff-breccia pipes, and were brought to the surface in the Hyblean Plateau (Sicily). Hyblean ultramafic xenoliths represent a suitable case-study, since they display widely serpentinized areas with blebs of condensed organic matter, due to abiotic synthesis. Interestingly, the organic matter contains tiny opaque carbonaceous flakes hosting clusters of nanodiamonds (Simakov et al., 2015).

2. Background

The Hyblean Plateau (Sicily, Southern Italy; Fig. 1) consists of a tectonically uplifted sedimentary and volcanic sequence cross-cut by a NE–SW-oriented system of extensional faults accommodated along a N–S trending, right-lateral transform fault zone (Fig. 1). A long and steep submarine slope, the "Hybla-Malta Escarpment", separates the eastern part of the Plateau from the Ionian abyssal plain. The exposed section of the Hyblean sedimentary sequence includes marine limestones and marls, Upper Cretaceous to Miocene in age, and Plio-Quaternary open-shelf clastics. Commercial boreholes reached Triassic carbonates, clayey deposits and basic igneous rocks at about 5 km b.s.l., even though geophysical data may suggest that the entire sequence is 8–10 km in thickness (Chironi et al., 2000). Basic volcanic rocks, representing a time interval from Upper Cretaceous to Pleistocene, crop out in different places of this area, especially in its northern part (Fig. 1).

A few nephelinitic diatremes, Upper Miocene in age (e.g. Carbone and Lentini, 1981; Suiting and Schminke, 2009) occur in the central part of the Plateau. The diatreme-filling breccia hosts a number of deep-seated xenoliths which consist of mantle-ultramafics and gabbros.

No outcrops, nor core-drill recovery of rocks from the pre-Triassic basement exist in the Hyblean Plateau as well as in the entire Central Mediterranean area. Seismic data, including tomography models, on the Hyblean Plateau and surrounding areas, can be either compatible with a serpentinized oceanic lithosphere (Manuella et al., 2013; Giampiccolo et al., 2017) or a strongly delaminated continental crust (Musumeci et al., 2014). Results of geological and paleontological investigations suggested that in the Late Permian the area corresponding to the present Sicily mainland, hence including the Hyblean sector, was located along a trans-Pangea seaway, connecting the western Tethys to Panthalassa through the present Mediterranean, the NW Africa offshore, and the Caribbean areas (Vai, 2003). The petrologic and geochemical investigation of the Hyblean deep-seated xenoliths validated the Vai's hypothesis (e.g. Manuella et al., 2015). In particular, Scribano et al. (2006a) found petrologic and geochemical evidence that the Hyblean oxide-rich tholeiite-gabbros, with sheared texture, closely resemble those drilled and dredged in modern oceanic core complexes (OCCs) along (ultra) slow-spreading oceanic ridges (e.g. Natland and Dick, 2001; Sharkov, 2012). Additionally, a set of petrographic evidence of abyssal-type hydrothermal metasomatism has been observed in many Hyblean xenoliths, including severe serpentinization of ultramafic rocks (Scribano et al., 2006b; Manuella, 2011). On these grounds, it is not a surprise that traces of hydrocarbons found in some hydrothermally altered gabbro and serpentinized ultramafic xenoliths (Ciliberto et al., 2009; Scirè et al., 2011) have been interpreted as abiotic organic compounds produced in the serpentinite basement via FT-t reactions.

3. Material and methods

The case-study sample is a strongly serpentinized and carbonated ultramafic rock extracted from the Valle Guffari tuff-breccia pipe (VG in Fig. 1), late Miocene in age, in the central part of the Hyblean Plateau

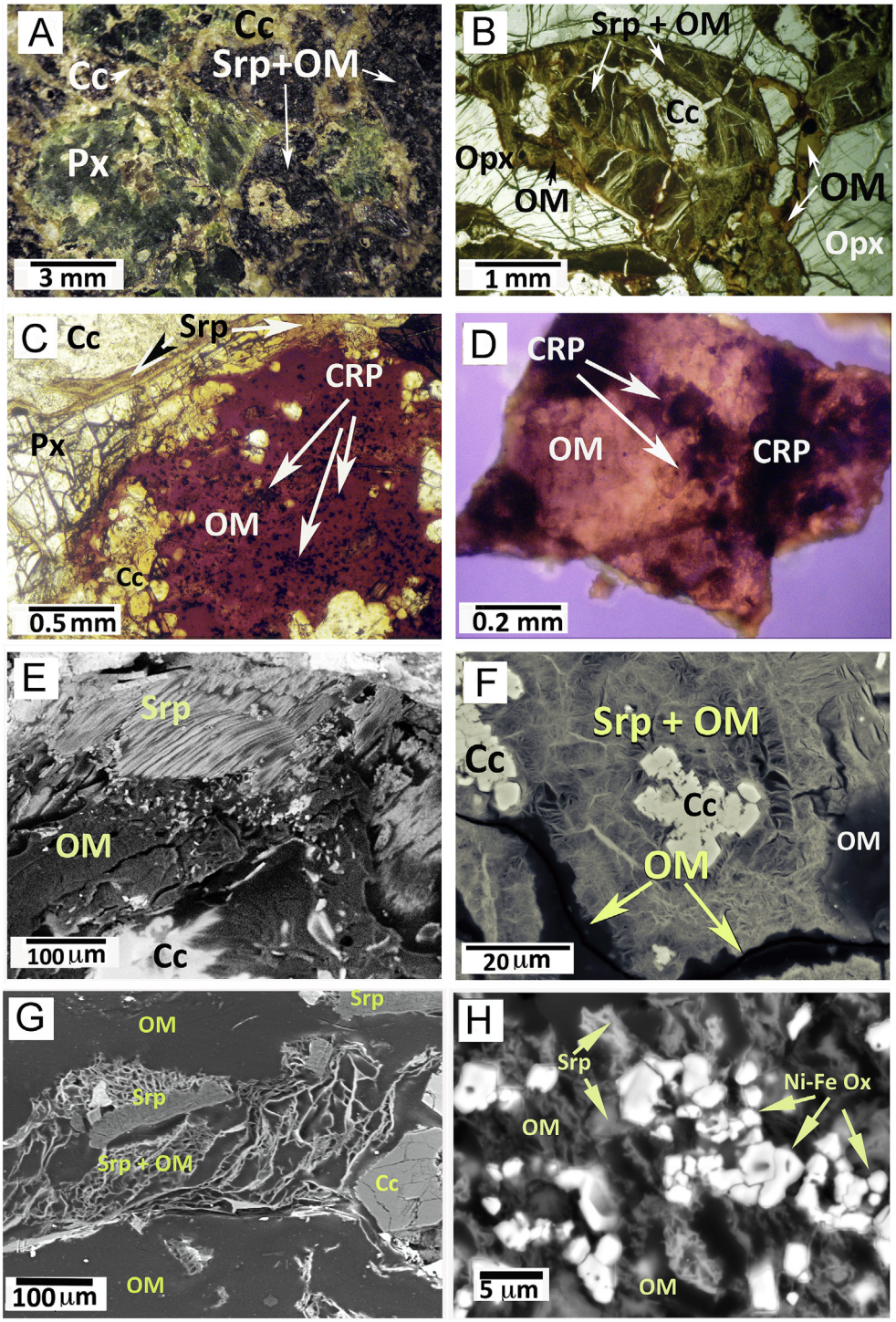

Fig. 2. Microphotographs displaying different aspects of the sample. (A) Magnified picture of a portion of the cut surface of the sample. (B) Portion of a thin section of the sample viewed under an optical microscope (plane-polarized transmitted light). Serpentine replaces former olivine, whereas organic matter (purplish) occurs either between serpentine fibers or as discrete blebs. (C) Detail of the same thin section highlighting clusters of black carbonaceous particles immersed in the purplish organic matter (plane-polarized transmitted light). (D) A thin slice of the raw organic matter as it appears under the optical microscope. Arrows indicate opaque patches consisting of clusters of diverse carbonaceous particles including nanodiamonds (detailed explanation in the text). (E) SEM image (BSE mode) of a portion of an uncoated thin section of the sample where serpentine, organic matter, and Ni-Fe oxide grains coexist (detailed explanation in the text). (F) SEM image of an uncoated thin section displaying the unusual textural relationships between fibrous serpentine and organic matter. (G) SEM image (BSE mode) of an uncoated fragment of the sample displaying serpentine, organic matter, and calcite. The arrow points to the zone viewed at higher magnification in the adjoining image (H). (H) High-magnification SEM image of the zone indicated by the arrow in (G), highlighting the relationships between organic matter and calcite grains (detailed explanation in the text). Legend: Px = pyroxenes; Opx = orthopyroxene; OM = organic matter; Srp = serpentine and coexisting talc, chlorite, and smectites; Cc = calcite; CRP = micrometric clusters of carbonaceous particles.

(Fig. 1). The sample has an ovoid shape, being about 12 cm × 8 cm × 6 cm in size.

The analytical methods related to previous investigations are reported in the related papers (Scirè et al., 2011; Simakov et al., 2015). Some data discussed in the present paper were newly acquired by the means of scanning electron microscope (SEM) and micro-Raman spectrometre. The used SEM was a TESCAN-VEGA\\LMU SEM equipped with an EDAX Neptune XM4 60 microanalysis working in energy dispersive spectrometry (EDS). Observations were made in backscattered electron mode under low vacuum conditions, on row fragments of the sample and on polished cut surfaces with no carbon coat. Quantitative analyses on silicate minerals were performed under high vacuum conditions at accelerating voltage 20 kV and beam current 0.2 nA, in carbon-coated polished thin sections.

Micro-Raman spectra on representative blebs of organic matter have been acquired with a Raman Jasco NRS-3100 apparatus at Catania University. The spectrometre was equipped with a microscope with ×10, ×20 and ×100 objectives. A laser excitation source at 532 nm was applied and the laser power was controlled by means of a series of density filters, in order to avoid heating effects. Depth resolution was set to few micrometres by means of a confocal hole. The system has been calibrated using the 520.7 cm^{-1} Raman band of silicon before each experimental

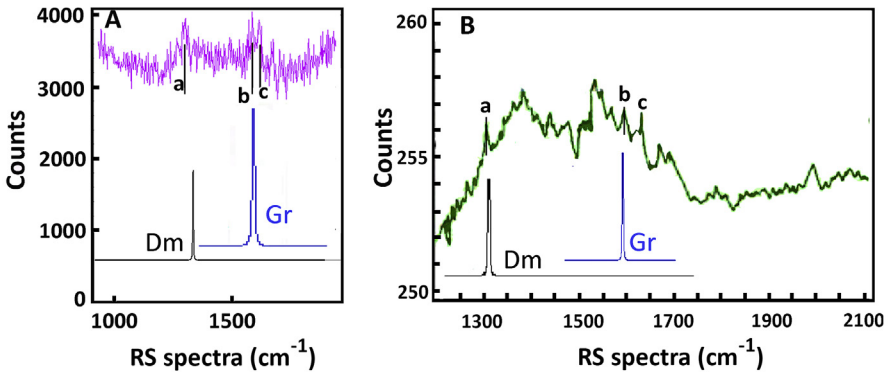

Fig. 3. Raman spectra of different portions of the sample. (A) RS spectra of an asphaltene sample obtained on a U-1000 spectrometer: (a) 1300 cm^{-1}, indicating the presence of nanodiamonds; (b) 1580 cm^{-1}; and (c) 1600 cm^{-1}, possibly indicating graphitic planes; (B) RS spectra of similar asphaltene sample obtained on a Jasco NRS-3100 spectrometer: (a) 1300–1312 cm^{-1}, indicating the presence of nanodiamonds; (b) 1576 cm^{-1}, (c) 1610 cm^{-1}, possibly indicating graphitic planes. Legend: Dm – RS spectra of diamond, Gr – RS spectra of graphite.

session. Raman (RS) and photoluminescence (PL) spectra were recorded on a U-1000 spectrometer with micro-Raman attachment at room temperature at Lebedev Physics Institute for the same blebs. Low-power excitation light (514.5 nm, <20 mW) was focused to a spot diameter of 10–40 μm. This allowed us to study the homogeneous and transition areas of the sample surface and monitor the absence of laser heating effect on the sample. The RS spectra were recorded with a resolution of 1–5 cm^{-1}. Since the Raman spectrum had a very low intensity, it was necessary to use a large time constant and subtraction of the luminescent background. Moreover, it was necessary to reduce the scan range (926−1938 cm^{-1}) in order to obtain a satisfactory signal-to-noise ratio.

4. Results

Petrologic and geochemical characteristics of the sample are synoptically reported in Table 1. Optical and SEM investigations (Fig. 2A) revealed that the sample consists of coarse pyroxene (enstatite and Cr-Al-diopside) and smaller Cr-Al-spinel grains immersed in a dominant assemblage of secondary minerals consisting of calcite and serpentine (lizardite), with minor talc, smectite, magnetite, trevorite, millerite, pyrite, Fe-sulfate, and Sn- and Pb-sulfides. No olivine is preserved in this rock as it has been fully replaced by serpentine (Fig. 2B). The primary spinel displays an oxidized outer rim. Pyroxene grains are locally crosscut by pressure cracks filled with secondary minerals. Clinopyroxene and serpentine are widely replaced by calcite.

Notably, the sample contains ~5 vol% of S-bearing asphaltene-like organic matter intermixed with serpentine fibers (Fig. 2D–F), forming discrete blebs and filling narrow cracks in the pyroxene grains and between grains (Fig. 2B). Furthermore, transmitted light observations, on standard thin-sections and thin speks of the unthreaded organic matter, revealed the abundance of micrometre-sized black (opaque) carbonaceous flakes (Fig. 2C and D) interspersed in the semi-transparent organic matter. HRTEM (high resolution transmission electron microscope) observations on the aforementioned black carbonaceous flakes showed (Simakov et al., 2015) that they contain aggregates of nanodiamonds mostly ranging from 1 nm to 6 nm. A few 10 nm-sized diamonds were also observed. This was the first clear evidence of the occurrence of nanodiamonds in a serpentinite. The infrared spectrum of residual black carbonaceous materials without silicates and soluble organic materials (treated asphaltene) indicated abundant aliphatic (CH_3 and CH_2) hydrocarbons and minor aromatic (C=C) hydrocarbons (Simakov et al., 2015). The stable carbon isotope values ($\delta^{13}C$) of the saturated and aromatic hydrocarbon fractions extracted from the asphaltene sample were −29.8‰ and −32.8‰, respectively. The $\delta^{13}C$ of the remaining solid residue (treated asphaltene) was −29.0‰ (Simakov et al., 2015).

4.1. New Raman investigation

Raman and photoluminescence spectra for two asphaltene blebs (A, B) containing black carbonaceous flakes display the following bands: 1287–1302 cm^{-1}, 1580 cm^{-1}, 1600 cm^{-1} (case "A", Figs. 3A) and 1300–1312 cm^{-1}, 1576 cm^{-1}, 1610 cm^{-1} (case "B", Fig. 3B). Bands at 1580–1600 cm^{-1} and 1576–1610 cm^{-1} may be due to the graphitic planes interconnected by sp^3 bonds (Karavanski et al., 2001). The ~1300 cm^{-1} bands can be attributed to nanodiamonds. From the obtained data, their frequency can be estimated as 1297 ± 10 cm^{-1} (Fig. 3A) and 1306 ± 6 cm^{-1} (Fig. 3B). The Raman line of fundamental oscillation experiences, as known, a low-frequency shift and asymmetric broadening with a decrease in the size of the crystals. This effect was explained on the basis of the phonon confinement model of Ager et al. (1991). Koniakhin et al. (2018) developed a new method, combining the dynamical matrix method (DMM) and the bond polarization model (BPM). Focusing on nanodiamond powders, the authors demonstrated that the DMM−BPM theory fits in the most recent experimental data much better than the commonly used phonon confinement model. Using the results of Koniakhin et al. (2018), it is therefore possible to roughly estimate the size of nanodiamonds in the studied carbonaceous flakes, being ~1.2 ± 0.2 nm and ~1.4 ± 0.2 nm, respectively. It cannot be excluded that larger nanodiamonds also coexist in different asphaltene blebs from the sample, as previous HRTEM investigation (Simakov et al., 2015) reported nanodiamonds ranging from 1 nm to 10 nm in size, with dominant size is ~6 nm.

5. Discussion

5.1. Origin of the organic matter and carbon particles

Scirè et al. (2011) described the multistage geologic history of the sample on the basis of its mineral assemblage. They also studied the organic matter by the means of micro-Fourier transform infrared spectra (μ-FTIR), X-ray photoelectron spectroscopy (XPS), thermo-gravimetric (TGA) and differential thermal analysis (DTA). They excluded that the organic matter could be infiltrated into the sample from an external source and concluded that it was a by-product of the serpentinization process that presumably occurred during the Early Triassic when the Hyblean uppermost mantle was tectonically exhumed at the Tethys Ocean seafloor (see Section 2). The serpentinization process in this region developed through time under different physic-chemical conditions; since its early stages, the conditions favored the formation of abiogenic hydrocarbons via FT-t synthesis. Fe-Ni alloys (e.g. awaruite) were putative catalysts of the FT-t synthesis, which, at a molecular scale, can be viewed as a catalyst-surface process (McCollom, 2013). The awaruite catalyst from the sample oxided to trevorite in the final stages of the serpentinization process (Scirè et al., 2011). At the final stage of serpentinization, the FT-t synthesis also yielded unsaturated hydrocarbons, including aromaticrings whose polycondensation gave rise to asphaltenes.

The secondary mineral assemblage in the sample suggested the presence of seawater-derived hydrothermal fluid with dissolved CO_2. Hence, based on the phase relationships in the $MgO\text{-}SiO_2\text{-}H_2O$ system (Evans, 2004; Klein and Bach, 2009), the detection of the lizardite

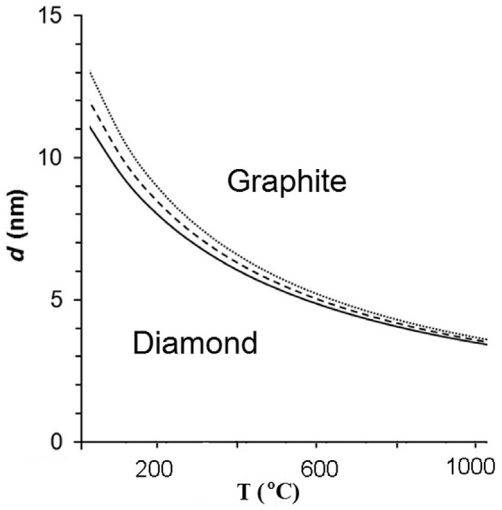

Fig. 4. Diamond-graphite dimensional curve from Manuella (2013) for *T-d* parameters (solid line – at normal pressure, dashed line – at 0.1 GPa, pointed line – at 0.2 GPa).

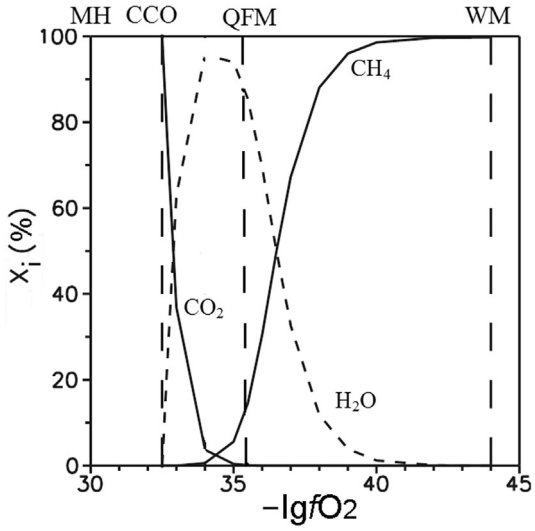

Fig. 5. Variation in the C–O–H system composition with oxygen fugacity at 300 °C and 2 kbar. MH: magnetite-hematite buffer; CCO: CO-CO_2-carbon buffer; QFM: quartz-magnetite-fayalite buffer; WM: wustite-magnetite buffer.

polytype by X-ray diffraction (XRD) suggests that the highest serpentinization temperature was ~300 °C (Scirè et al., 2011). On the other hand, the FTIR spectrum obtained using the attenuated total reflectance (ATR) method for the residual black carbonaceous materials indicates temperatures lower than 327 °C (Simakov et al., 2015).

The subsequent stages in the history of the sample's alteration were characterized by its incipient steatization, formation of clays after serpentine, and severe carbonatation of hydrocarbons and silicate minerals; these processes occurred at increasing $f(O_2)$ and $f(CO_2)$ conditions, hence decreasing $f(H_2)$ conditions. The occurrence of altered relict of spinel grains suggests that, in its earliest geologic history, the sample equilibrated in the upper mantle in the spinel-peridotite stability field, where graphite is the most stable carbon allotrope.

To summarize, an upper mantle volume consisting of nominally anhydrous, spinel-bearing, mantle peridotite veined by clinopyroxenite, was tectonically exhumed at a shallow sub-seafloor area of the slow-spreading Ionian Thetys Ocean presumably in the Early Triassic. There the ultramafic rocks interacted with a seawater-dominated hydrothermal fluid. In fact, the olivine and part of the orthopyroxene were transformed into serpentine, while the clinopyroxene was nearly unaffected.

The different generations of serpentine veins in the sample, along with their relationships with Fe-oxide and Fe-Ni sulfide micrograins, suggest that serpentinization developed in several stages at different temperatures. The $f(O_2)$ of the system evolved from reducing (i.e., below the quartz-fayalite-magnetite–QFM–buffer) to significantly oxidizing conditions (e.g. above the magnetite-hematite buffer), with the water/rock ratio increasing concomitantly through time. These circumstances can explain the oxidized outer rim of the primary spinel, along with the lack of primary sulfides (e.g. pentlandite), as opposed to the occurrence of millerite and pyrite, the latter showing alteration fringes into spongy magnetite and Fe-sulfate (Scirè et al., 2011). In this regard, the sulfur fugacity was probably in the range of $-1.8 < \log f(\Sigma S) < -0.6$, as suggested by the sulfide stability fields reported by Frost (1985). Moreover, an increasing $f(CO_2)$ through the geologic history of the sample is recorded by its extensive and pervasive carbonatation (Fig. 2A, D, G and H), which probably developed in different stages (Scirè et al., 2011).

5.2. Processes of nanodiamond formation

Some Raman-bands in the organic matter correspond, as mentioned, to diamonds of size 1–1.6 nm. Diamonds of the same size have been obtained by synthesis (Stehlik et al., 2015) and detected in meteorites (Daulton, 2006). In accordance with classification of Piekarczyk (1999) it corresponds to "higher diamondoids" formed in the temperature range of 150–350 °C at low pressure conditions (Dahl et al., 2003). Molecules of higher diamondoids (e.g. C_{22} and higher polymantanes) contain 4 to 11 diamond-crystal cages. The latter consist of 88 atoms, which corresponds to diamond sphere with diameter of nearly 1 nm. The octamantane class with formula $C_{34}H_{38}$ shows 18 isomeric structures with both chiral and achiral forms. All of these higher diamondoids correspond to nanometer-sized, H-terminated, diamonds of diverse shapes and sizes (Dahl et al., 2003). In accordance with the model of Badziag et al. (1990) they correspond to the transition of hydrocarbons to hydrogen terminated diamonds.

The studied nanodiamonds therefore correspond to the hydrogen-terminated polycrystalline CVD diamond reported by Landstrass and Ravi (1989), which can give rise to the crystalline interfacial water layers. Because of the surface energy, nanosized diamonds could be stable in the thermodynamic stability field of graphite. The size of the nanodiamonds is reported to decrease with increasing temperature (Gamarnik, 1996; Jiang et al., 2000; Manuella, 2013) (Fig. 4). Since there is no agreement between the results of the cited authors, it is not possible to extrapolate univocal temperature values which, however, are always compatible with the different stages of the serpentinization process (e.g. Evans, 2004; Klein and Bach, 2009).

We consider the following reaction for olivine hydration and formation of serpentine along with magnetite and dihydrogen:

$$3Fe_2SiO_4 + 3Mg_2SiO_4 + 6H_2O \rightarrow 2Mg_3Si_2O_5(OH)_4 + 2Fe_3O_4 + 2H_2 + 2SiO_2 \quad (2)$$

Taking into account the mineral assemblage in the sample and the phase relations reported by Evans (2004), we suggest that the initial $f(O_2)$ conditions were nearly the same as those of the quartz-magnetite-fayalite buffer. In fact, the lack of primary, high metal/S Ni-Fe sulfides in the sample (e.g. pentlandite) suggests an early desulfurization event with the probable formation of Ni-Fe alloys (e.g. awaruite; see previous section). This stage of the process is related to abiotic hydrocarbon synthesis via FT-type reactions. The temperature during this stage was presumably 300–150 °C.

In the CO_2-SiO_2-FeO-H_2O system, the following reaction is also possible.

$$6Fe_2SiO_4 + CO_2\ (aq) + 2H_2O \rightarrow 6SiO_2 + 4Fe_3O_4 + CH_4 \quad (3)$$

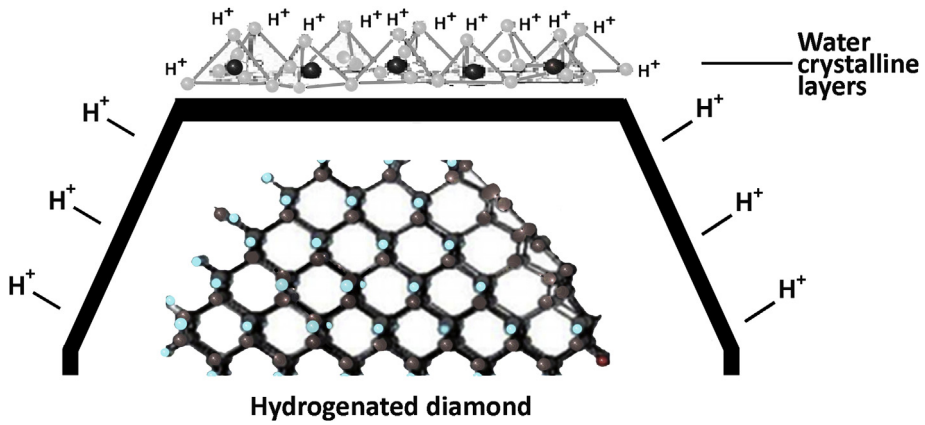

Fig. 6. The crystalline interfacial water layers on the diamond surface.

During the development of reactions (2 and 3), $f(H_2)$ increases and $f(O_2)$ decreases, corresponding to the transition from QFM to WM (wustite-magnetite) buffer. The composition of the C-O-H fluid system equilibrated with free carbon was calculated using the GFluid program (Zhang and Duan, 2010). This composition corresponds to water-rich fluid at the QFM buffer, and methane-rich fluid at the WM buffer (Fig. 5).

The transition from QFM to WM buffer has been put forward to explain, for example, the significant emission of hydrogen and methane over the ophiolitic zones (Schrenk et al., 2013). From the physic-chemical model of nanodiamond formation from fluid (Simakov, 2010) it follows that in those cases where hydrogen is much more abundant than methane, in the H–C system, the formation of nanodiamonds is possible by the reaction:

$$CH_4 \rightarrow C + 2H_2 \quad (4)$$

The serpentinization reaction in WM buffer conditions resulted in the full replacement of olivine, partial replacement of orthopyroxene, and formation of hydrocarbons (presumably alkanes; e.g. Ciliberto et al., 2009) along with the majority of the free nanocarbons (nanodiamond and graphite). The 6-nm diamonds were realistically formed during these processes. As a result, carbon was immersed in the hydrocarbon medium (Fig. 2C), protecting nanocarbons from late replacement by carbonate. On these grounds, it is opportune to note that the carbon isotopic results obtained in the serpentinite (see previous section) are consistent with the isotopic data of methane formed in hydrothermal systems. For example, Etiope and Schoell (2014) reported a set of $\delta^{13}C$ values between −32‰ and−30‰, similar to the sample values, in gaseous hydrocarbon seepage from serpentinizing ultramafic rocks in the Othyris Ophiolite complex (Greece). This confirms the shallow hydrocarbon sources of the nanocarbon formation in the serpentinite.

Diamond nuclei formation is possible also (Simakov, 2010) from H_2O-CO_2-rich fluids containing minor CH_4 contents which corresponds to the region of $f(O_2)$ between CCO (upper limit of carbon stability) and QFM buffers (Fig. 5). Rudenko et al. (1993) indicated that diamond could be formed under such a chemical condition by the reaction of methane and carbon dioxide:

$$CH_4 + CO_2 \rightarrow 2C + 2H_2O \quad (5)$$

At higher temperatures the formation of micrometre-sized diamonds is possible in the serpentinization processes of ultramafic rocks (Farré-de-Pablo et al., 2018). The micrometre-sized diamonds could be formed here from hydrocarbon fluids by reactions (4) and (5) at supercritical water conditions (Simakov, 2018). On nowadays several scientific groups from different countries have independently confirmed the existence of diamonds in ophiolites (Yang et al., 2014, 2015, 2020 and references therein).

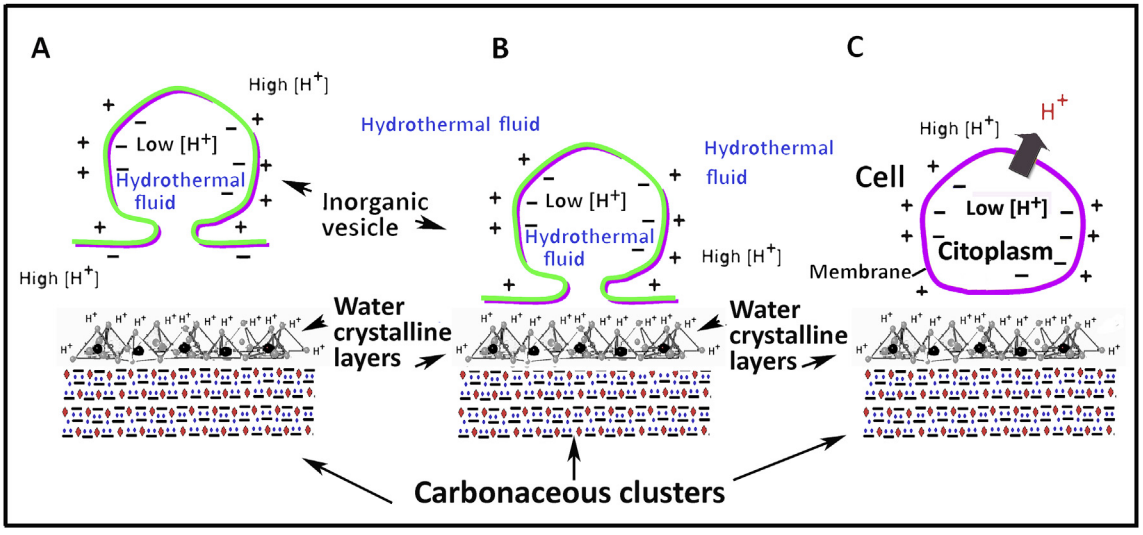

Fig. 7. Scheme of cell formation in accordance with model of Lane et al. (2010). (A) The initial stage of cell formation: Proton-motive force exists across the boundary of LUCA in hydrothermal fluid. (B) The middle stage of cell formation: Proton-motive force exists across the boundary of LUCA on the seed of hydrogenated carbon clusters in the hydrothermal fluid. (C) The final stage of cell formation: Proton-motive force of living cells finally forming from LUCA. (In the clusters red diamonds – nanodiamonds, black tire – nanographite, blue point – organics).

5.3. Mineral surfaces as key factors for abiogenesis

Pyrite in the sample is most probably related to the circulation of S-rich hydrothermal fluids, at moderate temperature conditions ($T < 350$ °C), as suggested by relevant experimental data (e.g. Shock, 1992). In a later stage of the hydrothermal system geological history, dramatic variation of physic-chemical parameters, such as a significant increase in the water/rock ratio, induced desulfidization, hence pyrite grains were extensively replaced by Fe-oxides which mainly consist of magnetite (Scribano et al., 2019), according, for example, to the following reaction (Qian et al., 2010):

$$3FeS_2\ (s) + 6H_2O = Fe_3O_4\ (s) + 6H_2S\ (aq) + O_2\ (g) \quad (6)$$

More precisely, pyrite dissolution kinetics can be described in term of an electrochemical mechanism. The anodic reaction produces ferrous and sulfate ions (Caldeira et al., 2010):

$$FeS_2 + 8H_2O = Fe^{2+} + 2SO_4^{2-} + 16H^+ + 14e^- \quad (7)$$

Reactions (6 and 7), and possibly others, can create favorable conditions for the onset of chemiosmotic processes and proton gradients in the alkaline hydrothermal vents. The hydrated nanodiamonds, as it was noted before, are good media for proton transporting because diamond surface could create the crystalline interfacial water layers (Fig. 6). Certainly there are yet a lot of missing pieces in such an extremely complex puzzle consisting of the formation, at $T < 100$ °C, of 'LUCA' structures (Last Universal Common Ancestor of cells; Lane et al., 2010). RNA, DNA, the universal genetic code, transcription, translation, ribosomes, a rotor-stator-type ATPase, ATP and the Krebs cycle in all living organisms could be inherited from LUCA (Lane et al., 2010). The proton-motive force is made by analkaline (high pH) internal effluent from LUCA's founding hydrothermal vent and an acidic (low pH) external environment of carbonic acid solution (Fig. 7A). At this stage, hydrogen could be outgassed from nanodiamonds (Landstrass and Ravi, 1989), and create the high [H^+] layer on cluster surfaces. The transformation of the LUCA structure to the living cell might have been possible on the surface of the carbonaceous cluster, including nanodiamonds, due to the high pH in the surrounding fluid medium (Fig. 7b). As a result, an electron flow across the "membrane" from donors to acceptors is set up, likewise it occurs in living cells (Fig. 7c).

6. Conclusions

The finding of carbonaceous flakes with clusters of hydrogenated nanodiamonds dispersed in blebs of condensed abiotic organic matter in a serpentinite xenolith from the Hyblean area, supports the hypothesis of the prebiotic relevance of the several reactions occurring in abyssal serpentinite systems in the prebiotic Earth (Dodd et al., 2017). In fact, the carbonaceous clusters with dissolved hydrogen layers can give rise to high [H^+] abundance also forming inner organics crystalline water layers on the nanodiamond surfaces (Sommer et al., 2008). In addition, the presence of sulfide minerals in the sample may be related to chemiosmotic processes, hence to proton gradients. Both nanodiamond clusters and sulfide minerals are therefore capable of stimulating the formation of different prebiotic compounds necessary, even though not sufficient, to the formation of 'LUCA' (Last Universal Common Ancestor) structure in the early Earth (Lane et al., 2010).

Declaration of competing interest

The authors declare that they have no known competing financial interests or personal relationships that could have appeared to influence the work reported in this paper.

Acknowledgements

Constructive comments by three anonymous Reviewers are gratefully acknowledged.

References

Ager, J.W., Veirs, D.K., Rosenblat, G.M., 1991. Spatially resolved Raman studies of diamond films grown by chemical vapor deposition. Phys. Rev. B43, 6491–6499.
Angus, J.S., Hayman, C.C., 1988. Low-pressure metastable growth of diamond and "diamond-like" phases. Science 241, 913–921.
Badziag, P., Verwoerd, W.S., Ellis, W.P., Greimer, N.R., 1990. Nanometer-sized diamonds are more stable than graphite. Nature 343, 244–245.
Bauschlicher Jr., C.W., Liu, Y.F., Ricca, A., Mattioda, A.L., Allamandola, L.J., 2007. Electronic and vibration spectroscopy of diamondoids and the interstellar infrared bands between 3.35 and 3.55 μm. Astrophys. J. 671, 458–469.
Baymann, F., Lebrun, E., Brugna, M., Schoepp-Cothenet, B., Giudici-Orticoni, M.T., Nitschke, W., 2003. The redox protein construction kit: pre-last universal common ancestor evolution of energy conserving enzymes. Philos. Trans. R. Soc. Lond. Ser. B Biol. Sci. 358, 267–274.
Bebié, J., Schoonen, M.A.A., 2000. Pyrite surface interaction with selected organic aqueous species under anoxic conditions. Geochem. Trans. 8, 1–7.
Blöchl, E., Keller, M., Wachtershäuser, G., Stetter, K.O., 1992. Reactions depending on iron sulfide and linking geochemistry with biochemistry. Proc. Natl. Acad. Sci. U. S. A. 89, 8117–8120.
Brazelton, W.J., Mehta, M.P., Kelley, D.S., Baross, J.A., 2011. Physiological differentiation within a single-species biofilm fueled by serpentinization. mBio 2, e00127–11. https://doi.org/10.1128/mBio.00127-11.
Caldeira, C.L., Ciminelli, V.S.T., Osseo-Asare, K., 2010. The role of carbonate ions in pyrite oxidation in aqueous systems. Geochem. Cosmochim. Acta 74, 1777–1789.
Carbone, S., Lentini, F., 1981. Caratteri deposizionali delle vulcaniti del Miocene superiore negli Iblei (Sicilia sud-orientale). Geologica Romana 20, 79–101 (in Italian with English abstract).
Chironi, C., De Luca, L., Guerra, I., Lizio, D., Moretti, A., Vitale, M., 2000. Crustal structures of the Southern Tyrrhenian sea and Sicily channel on the basis of the M25, M26, M28, M39, WARR profiles. Ital. J. Geosci. 119, 189–203.
Ciliberto, E., Crisafulli, C., Manuella, F.C., Samperi, F., Scirè, S., Scribano, V., Viccaro, M., Viscuso, E., 2009. Aliphatic hydrocarbons in metasomatized gabbroic xenoliths from Hyblean diatremes (Sicily): genesis in a serpentinite hydrothermal system. Chem. Geol. 258, 258–268.
Dahl, J.E., Liu, S.G., Carlson, R.M.K., 2003. Isolation and structure of higher diamondoids, nanometer-sized diamond molecules. Science 299, 96–99.
Dai, Z.R., Bradley, J.P., Joswiak, D.J., Brownlee, D.E., Hill, H.G., Genge, M.J., 2002. Possible in situ formation of meteoritic nanodiamonds in the early Solar System. Nature 418, 157–159.
Daulton, T., 2006. Extraterrestrial nanodiamonds in the cosmos. In: Shenderova, O.A., Gruen, D.M. (Eds.), Ultrananocrystalline Diamond: Synthesis, Properties, and Applications. William Andrew Publishing, Elsevier, New York, pp. 23–78.
Dodd, M.S., Papineau, D., Grenne, T., Slack, J.F., Rittner, M., Pirajno, F., O'Neil, J., Little, C.T.S., 2017. Evidence for early life in Earth's oldest hydrothermal vent precipitates. Nature 543, 60–64.
Etiope, G., Schoell, M., 2014. Abiotic gas: atypical, but not rare. Elements 10, 201–296.
Evans, B.W., 2004. The serpentinite multisystem revisited: chrysotile is metastable. Int. Geol. Rev. 46, 479–506.
Farré-de-Pablo, J., Proenza, J.A., González-Jiménez, J.M., Garcia-Casco, A., Colás, V., Roqué- Rossell, J., Camprubí, A., Sánchez-Navas, A., 2018. A shallow origin for diamonds in ophiolitic chromitites. Geology 47, 75–78.
Fedoseev, D.V., Varnin, V.P., Deryagin, B.V., 1984. Diamond synthesis in the field of its thermodynamic metastability. Russ. Chem. Rev. 53, 753–771.
Frost, R.B., 1985. On the stability of sulphides, oxides, and native metals in serpentinite. J. Petrol. 26, 31–63.
Galli, G., 2010. Structure, stability and electronic properties of nanodiamonds. In: Colombo, L., Fasolino, A. (Eds.), Computer-Based Modeling of Novel Carbon Systems and Their Properties. Springer, pp. 37–56.
Gamarnik, M.Y., 1996. Energetical preference of diamond nanoparticles. Phys. Rev. B 54, 2150–2156.
Giampiccolo, E., Brancato, A., Manuella, F.C., Carbone, S., Gresta, S., Scribano, V., 2017. New evidence for the serpentinization of the Palaeozoic basement of southeastern Sicily from joint 3-D seismic velocity and attenuation tomography. Geophys. J. Int. 211, 1375–1395.
Hazen, R.M., Sverjensky, D.A., 2010. Mineral surfaces geochemical complexities and the origins of life. Cold Spring Harbor Perspect. Biol. 2, a002162.
Holm, N.G., Ertem, G., Ferris, J.P., 1993. The binding and reactions of nucleotides and polynucleotides on iron oxide hydroxide polymorphs. Orig. Life Evol. Biosph. 23, 195–215.
Jiang, Q., Li, J.C., Wilde, G., 2000. The size dependence of the diamond-graphite transition. J. Phys. Condens. Matter 12, 5623–5627.
Karavanski, V.A., Mel'Nik, N.N., Zavaritskaya, T.N., 2001. Preparation and study of the optical properties of porous graphite. JETP Lett. (Engl. Transl.) 74, 186–189.

Klein, F., Bach, W., 2009. Fe-Ni-Co-O-S phase relations in peridotite-seawater interactions. J. Petrol. 50, 37–59.
Koniakhin, S.V., Utesov, O.I., Terterov, I.N., Siklitskaya, A.V., Yashenkin, A.G., Solnyshkov, D., 2018. Raman spectra of crystalline nanoparticles: replacement for the phonon confinement model. J. Phys. Chem. C 122, 19219–19229.
Konn, C., Charlou, J.L., Donval, J.P., Holm, N.G., Dehairs, F., Bouillon, S., 2009. Hydrocarbons and oxidized organic compounds in hydrothermal fluids from Rainbow and Lost City ultramafic-hosted vents. Chem. Geol. 258, 299–314.
Kouchi, A., Nakano, H., Kimura1, Y., Kaito, C., 2005. Novel routes for diamond formation in interstellar ices and meteoritic parent bodies. Astrophs. J. 626, L129–L132.
Landstrass, M.I., Ravi, K.V., 1989. Resistivity of chemical vapour deposited diamond films. Appl. Phys. Lett. 55, 975–977.
Lane, N., Allen, J.F., Martin, W., 2010. How did LUCA make a living? Chemiosmosis in the origin of life. Bioessays 32, 271–280.
Manuella, F.C., 2011. Vein mineral assemblage in partially serpentinized peridotite xenoliths from Hyblean Plateau (Southeastern Sicily, Italy). Period. Mineral. 80, 247–266.
Manuella, F.C., 2013. Can nanodiamonds grow in serpentinite-hosted hydrothermal systems? A theoretical modelling study. Mineral. Mag. 77, 3163–3174.
Manuella, F.C., Brancato, A., Carbone, S., Gresta, S., 2013. A crustal–upper mantle model for southeastern Sicily (Italy) from the integration of petrologic and geophysical data. J. Geodyn. 66, 92–102.
Manuella, F.C., Scribano, V., Carbone, S., Brancato, A., 2015. The Hyblean xenolith suite (Sicily): an unexpected legacy of the Ionian–Tethys realm. Int. J. Earth Sci. 104, 1317–1336.
Matsumoto, S., Sato, Y., Kamo, M., Setaka, N., 1982. Vapor deposition of diamond particles from methane. Jpn. J. Appl. Phys. 21, L183–L185.
McCollom, T.M., 2013. Laboratory simulations of abiotic hydrocarbon formation in Earth's deep subsurface. Rev. Mineral. Geochem. 75, 467–494.
McCollom, T.M., Seewald, J.S., 2013. Serpentinites, hydrogen, and life. Elements 9, 129–134.
Menéz, B., Pisapia, C., Andreani, M., Jamme, F., Vanbellingen, Q.P., Brunelle, A., Richard, L., Dumas, P., Réfrégiers, M., 2018. Abiotic synthesis of amino acids in the recesses of the oceanic lithosphere. Nature 564, 59–63.
Musumeci, C., Scarfì, L., Palano, M., Patanè, D., 2014. Foreland segmentation along an active convergent margin: new constraints in southeastern Sicily (Italy) from seismic and geodetic observations. Tectonophysics 630, 137–149.
Nakano, H., Kouchi, A., Tachibana, S., Tsuchiyama, A., 2002. Evaporation of interstellar organic materials in the solar nebula. Astrophys. J. 592, 1252–1262.
Natland, J.H., Dick, H.J.B., 2001. Formation of the lower ocean crust and the crystallization of gabbroic cumulates at a very slowly spreading ridge. J. Volcanol. Geoth. Res. 110, 191–233.
Nekhaev, A.I., Bagrii, E.I., Maximov, A.L., 2011. Petroleum nanodiamonds: new in diamondoid naphthenes. Petrol. Chem. 51, 86–95.
Piekarczyk, W., 1999. Crystal growth of CVD diamond and some of its peculiarities. Cryst. Res. Technol. 34, 553–563.
Qian, G., Brugger, F., Skinner, W.M., Chen, G., Pring, A., 2010. An experimental study of the mechanism of the replacement of magnetite by pyrite up to 300 °C. Geochem. Cosmochim. Acta 74, 5610–5630.
Ristein, J., 2001. Electron affinities of diamond surface. In: Nazarer, M.H., Neves, A.J. (Eds.), Properties, Growth and Applications of Diamond. Inspec, London, pp. 73–75.
Rudenko, A.P., Kulakova, I.I., Skvortsova, V.L., 1993. The chemical synthesis of diamond. Aspects of the general theory. Russ. Chem. Rev. 62, 87–104.
Russel, M.J., Hall, A.J., Boyce, A.J., Fallick, A.E., 2005. On hydrothermal convection systems and the emergence of life. Econ. Geol. 100, 419–438.
Schrenk, M.O., Brazelton, W.J., Lang, S.Q., 2013. Serpentinization, carbon, and deep life. Rev. Mineral. Geochem. 75, 575–606.
Schulte, M.D., Rogers, K.L., 2004. Thiols in hydrothermal solution: standard partial molal properties and their role in the organic geochemistry of hydrothermal environments. Geochem. Cosmochim. Acta 68, 1087–1097.
Scirè, S., Ciliberto, E., Crisafulli, C., Scribano, V., Bellatreccia, F., Ventura, G.D., 2011. Asphaltene-bearing mantle xenoliths from Hyblean diatremes, Sicily. Lithos 125, 956–968.
Scribano, V., Sapienza, G.T., Braga, R., Morten, L., 2006a. Gabbroic xenoliths in tuff-breccia pipes from the Hyblean Plateau: insights into the nature and composition of the lower crust underneath Southeastern Sicily. Ital. Mineral. Petrol. 86, 63–88.
Scribano, V., Ioppolo, S., Censi, P., 2006b. Chlorite/smectite-alkali feldspar metasomatic xenoliths from Hyblean Miocenic diatremes (Sicily, Italy): evidence for early interaction between hydrothermal brines and ultramafic/mafic rocks at crustal levels. Ofioliti 31, 161–171.
Scribano, V., Simakov, S.K., Finocchiaro, C., Correale, A., 2019. Pyrite and organic compounds coexisting in intrusive mafic xenoliths (Hyblean Plateau, Sicily): implications for subsurface abiogenesis. Orig. Life Evol. Biosph. 49, 19–47.
Sharkov, E.V., 2012. Cyclic development of axial parts of slow-spreading ridges: evidence from Sierra Leone area, the mid-atlantic ridge, 5-7°N. In: Sharkov, E.V. (Ed.), Tectonics, Recent Advances. Chapter: 1. InTech, Rijeka, pp. 3–36. https://doi.org/10.5772/39372.
Shock, E.L., 1992. Chemical environments in submarine hydrothermal systems. In: Holm, N.G. (Ed.), Marine Hydrothermal Systems and the Origin of Life. Springer, Dordrecht, The Netherlands, pp. 67–107.
Simakov, S.K., 2010. Metastable nanosized diamond formation from C-H-O fluid Sistem. J. Mater. Res. 25, 2336–2340.
Simakov, S.K., 2018. Nano- and micron-sized diamond genesis in nature: an overview. Geosci. Front. 9, 1849–1858.
Simakov, S.K., Kouchi, A., Mel'nik, N.N., Scribano, V., Kimura, Y., Hama, T., Suzuki, N., Saito, H., Yoshizawa, T., 2015. Nanodiamond finding in the Hyblean shallow mantle xenoliths. Sci. Rep. 5, 10765. https://doi.org/10.1038/srep10765.
Sommer, A.P., Zhu, D., Fecht, H.-J., 2008. Genesis on diamonds. Cryst. Growth Des. 8, 2628–2629.
Spitsyn, R.V., Bouilov, L.L., Deryagin, B.V., 1981. Vapor growth of diamond on diamond and other surfaces. J. Cryst. Growth 52, 219–226.
Stehlik, S., Varga, M., Ledinsky, M., Jirasek, V., Artemenko, A., Kozak, H., Ondic, L., Skakalova, V., Argentero, G., Pennycook, T., Meyer, J.C., Fejfar, A., Kromka, A., Rezek, B., 2015. Size and purity control of HPHT nanodiamonds down to 1 nm. J. Phys. Chem. C 119, 27708–27720.
Suiting, I., Schmincke, H.U., 2009. Internal vs. external forcing in shallow marine diatreme formation: a case study from the Iblean Mountains (SE-Sicily, Central Mediterranean). J. Volcanol. Geoth. Res. 186 (3), 361–368.
Szent-Gyorgyi, A., 1971. Biology and pathology of water. Perspect. Biol. Med. 14, 239–249.
Tielens, A.G.G.M., Seab, C.G., Hollenbach, D.J., McKee, C.F., 1987. Shock processing of interstellar dust-Diamonds in the sky. Astrophys. J. 319, L109–L113.
Vai, G.B., 2003. Development of the palaeogeography of Pangaea from Late Carboniferous to Early Permian. Palaeogeogr. Palaeoclimatol. Palaeoecol. 196, 125–155.
Wang, Z.H., Xie, X.H., Xiao, S.M., Liu, J.S., 2010. Adsorption behavior of glucose on pyrite surface investigated by TG, FTIR and XRD analyses. Hydrometallurgy 102, 87–90.
Webb, S.J., 1965. Bound Water in Biological Integrity. C.C. Thomas, Springfield, Ill.
Yang, J.S., Robinson, P.T., Dilek, Y., 2014. Diamonds in ophiolites. Elements 10, 127–130.
Yang, J.S., Meng, F., Xu, X., Robinson, P.T., Dilek, Y., Makeyev, A.B., Wirth, R., Wiedenbeck, M., Cliff, J., 2015. Diamonds, native elements and metal alloys from chromitites of the Ray-Iz ophiolite of the Polar Urals. Gondwana Res. 27, 459–485.
Yang, J.S., Simakov, S.K., Moe, K.S., Scribano, V., Lian, D., Wu, W., 2020. Comment on "Comparison of enigmatic diamonds from the Tolbachik arc volcano (Kamchatka) and Tibetan ophiolites: assessing the role of contamination by synthetic materials" by Litasov et al. (2019). Gondwana Res. 79, 301–303.
Zhang, C., Duan, Z.H., 2010. GFluid: an Excel spreadsheet for investigating C–O–H fluid composition under high temperatures and pressures. Comput. Geosci. 36, 569–572.